Magnetic Oscillation of Optical Phonon in Graphene

Tsuneya ANDO

Department of Physics, Tokyo Institute of Technology
2–12–1 Ookayama, Meguro-ku, Tokyo 152-8551

The frequency shift and broadening of long-wavelength optical phonons due to interactions with electrons are calculated in a monolayer graphene in magnetic fields. The broadening is resonantly enhanced and the frequency shift exhibits a rapid change when the phonon energy becomes the energy separation of Landau levels between which optical transitions are allowed.

Keywords: two-dimensional graphite, electron-phonon interaction, optical phonon, broadening

§1. Introduction

In a monolayer graphene, the phonon spectrum can be modified directly by the change in the electron or hole concentration by a gate voltage. In particular the phonon frequencies near the Γ point can be measured directly by the Raman scattering.[1,2] In a previous work,[3] this electron-concentration dependence of the frequency and the broadening of optical phonons were investigated in the absence of a magnetic field. In this paper we shall study effects of magnetic field.

In an effective-mass approximation, an electron in a graphite monolayer is described by Weyl's equation for a massless neutrino.[4,5] Transport properties in such an exotic electronic structure are quite intriguing, and the conductivity with/without a magnetic field including the Hall effect[6,7] and the dynamical transport[8] were investigated theoretically. The results show that the system exhibits various characteristic behaviors different from conventional two-dimensional systems.[9] Quite recently, this single layer graphite was fabricated,[10] and the magnetotransport was measured including the integer quantum Hall effect, demonstrating the validity of the neutrino description of the electronic states.[11,12] Since then, the graphene became the subject of extensive theoretical[13−20] and experimental study.[21,22]

For graphene and carbon nanotubes, a continuum model suitable for a correct description of long-wavelength acoustic phonons was constructed,[23] and a similar continuum model was developed for optical phonons and the Hamiltonian for electron-phonon interactions was derived also.[24] We shall use this continuum model to calculate the self-energy of phonon Green's function in graphene in magnetic fields. The real part of the self-energy gives an energy shift and the imaginary part provides a lifetime.

The paper is organized as follows: In §2, electronic states in a magnetic field and a continuum model of optical phonons are reviewed very briefly. The phonon Green's function is calculated and shifts and broadening of phonon modes are discussed in §3. Some examples of numerical results are presented and discussed in §4 and a short summary is given in §5.

§2. Formulation

2.1 Effective-mass description

In a graphite sheet the conduction and valence bands consisting of π orbitals cross at K and K' points of the Brillouin zone, where the Fermi level is located.[25,26] Electronic states of the π-bands near a K point in magnetic field B perpendicular to the sheet are described by the $\boldsymbol{k}\cdot\boldsymbol{p}$ equation:[4−5]

$$\mathcal{H}_0\boldsymbol{F}(\boldsymbol{r}) = \varepsilon\boldsymbol{F}(\boldsymbol{r}), \tag{2.1}$$

with

$$\mathcal{H}_0 = \gamma\begin{pmatrix} 0 & \hat{k}_x - \mathrm{i}\hat{k}_y \\ \hat{k}_x + \mathrm{i}\hat{k}_y & 0 \end{pmatrix} = \gamma(\boldsymbol{\sigma}\cdot\boldsymbol{k}), \tag{2.2}$$

where γ is a band parameter, $\boldsymbol{\sigma} = (\sigma_x, \sigma_y)$ is the Pauli spin matrix, and $\hat{\boldsymbol{k}} = (\hat{k}_x, \hat{k}_y) = -\mathrm{i}\boldsymbol{\nabla} + e\boldsymbol{A}/\hbar c$ is a wave-vector operator, with the vector potential $\boldsymbol{A} = (Bx, 0)$ in magnetic field B perpendicular to the system.

The wave function is written as

$$\boldsymbol{F}_{nX}(\boldsymbol{r}) = \frac{C_n}{\sqrt{L}}\exp\Big(-\mathrm{i}\frac{Xy}{l^2}\Big)\begin{pmatrix} \mathrm{sgn}(n)h_{|n|-1}(x-X) \\ h_{|n|}(x-X) \end{pmatrix}, \tag{2.3}$$

with

$$C_n = \begin{cases} 1 & (n=0)\ , \\ \dfrac{1}{\sqrt{2}} & (n\neq 0)\ , \end{cases} \tag{2.4}$$

$$\mathrm{sgn}(n) = \begin{cases} 1 & (n>0)\ , \\ 0 & (n=0)\ , \\ -1 & (n<0)\ , \end{cases} \tag{2.5}$$

$$h_{|n|}(x) = \frac{\mathrm{i}^{|n|}}{\sqrt{2^{|n|}|n|!\sqrt{\pi}l}}\exp\Big[-\frac{1}{2}\Big(\frac{x}{l}\Big)^2\Big]H_{|n|}\Big(\frac{x}{l}\Big), \tag{2.6}$$

where L is the linear dimension of the system, X is a center coordinate, $H_n(t)$ is the Hermite polynomial, $l = \sqrt{c\hbar/eB}$, and $n = 0, \pm1, \ldots$. The corresponding energy is given by

$$\varepsilon_n = \mathrm{sgn}(n)\hbar\omega_B\sqrt{|n|}, \tag{2.7}$$

with effective magnetic energy given by

$$\hbar\omega_B = \frac{\sqrt{2}\gamma}{l}. \tag{2.8}$$

States are specified by a set of quantum numbers $\alpha = (n, X)$. We shall neglect a small spin-Zeeman splitting

in this paper.

For the K' point, the Hamiltonian is given by

$$\mathcal{H}_0 = \gamma \begin{pmatrix} 0 & \hat{k}_x + \mathrm{i}\hat{k}_y \\ \hat{k}_x - \mathrm{i}\hat{k}_y & 0 \end{pmatrix} = \gamma(\boldsymbol{\sigma}^* \cdot \hat{\boldsymbol{k}}), \tag{2.9}$$

and the corresponding wave function is given by

$$\boldsymbol{F}_{nX}(\boldsymbol{r}) = \frac{C_n}{\sqrt{L}} \exp\Bigl(-\mathrm{i}\frac{Xy}{l^2}\Bigr) \begin{pmatrix} h_{|n|}(x-X) \\ \mathrm{sgn}(n) h_{|n|-1}(x-X) \end{pmatrix}. \tag{2.10}$$

The presence of the Landau level $\varepsilon_0 = 0$ is attributed to Berry's phase due to a rotation in the $\boldsymbol{k}$ space around the origin.

2.2 Long Wavelength Optical Phonon

The long-wavelength optical phonons in the two-dimensional graphite was discussed previously based on a valence-force-field model,[23,24] and in the following we shall limit ourselves to the long-wavelength limit. Optical phonons are represented by the relative displacement of two sub-lattice atoms A and B,

$$\boldsymbol{u}(\boldsymbol{r}) = \sum_{\boldsymbol{q},\mu} \sqrt{\frac{\hbar}{2NM\omega_0}} (b_{\boldsymbol{q}\mu} + b^\dagger_{-\boldsymbol{q}\mu}) \boldsymbol{e}_\mu(\boldsymbol{q}) \mathrm{e}^{\mathrm{i}\boldsymbol{q}\cdot\boldsymbol{r}}, \tag{2.11}$$

where N is the number of unit cells, M is the mass of a carbon atom, ω_0 is the phonon frequency at the Γ point, $\boldsymbol{q} = (q_x, q_y)$ is the wave vector, μ denotes the modes (t for transverse and l for longitudinal), and $b^\dagger_{\boldsymbol{q}\mu}$ and $b_{\boldsymbol{q}\mu}$ are the creation and destruction operators, respectively. Define

$$q_x = q\cos\varphi(\boldsymbol{q}), \quad q_y = q\sin\varphi(\boldsymbol{q}), \tag{2.12}$$

with $q = |\boldsymbol{q}|$. Then, we have

$$\begin{aligned} \boldsymbol{e}_\mathrm{l}(\boldsymbol{q}) &= \mathrm{i}(\cos\varphi(\boldsymbol{q}), \sin\varphi(\boldsymbol{q})), \\ \boldsymbol{e}_\mathrm{t}(\boldsymbol{q}) &= \mathrm{i}(-\sin\varphi(\boldsymbol{q}), \cos\varphi(\boldsymbol{q})). \end{aligned} \tag{2.13}$$

The corresponding phonon Hamiltonian is written as

$$\mathcal{H}_\mathrm{ph} = \sum_{\boldsymbol{q},\mu} \hbar\omega_0 \Bigl(b^\dagger_{\boldsymbol{q}\mu} b_{\boldsymbol{q}\mu} + \frac{1}{2}\Bigr). \tag{2.14}$$

The interaction between optical phonons and an electron at the K point is given by[24]

$$\mathcal{H}^\mathrm{K}_\mathrm{int} = -\sqrt{2}\frac{\beta\gamma}{b^2} \boldsymbol{\sigma} \times \boldsymbol{u}(\boldsymbol{r}), \tag{2.15}$$

and for the K' point

$$\mathcal{H}^{\mathrm{K}'}_\mathrm{int} = -\sqrt{2}\frac{\beta\gamma}{b^2} \boldsymbol{\sigma}^* \times \boldsymbol{u}(\boldsymbol{r}), \tag{2.16}$$

where the vector product for vectors $\boldsymbol{a} = (a_x, a_y)$ and $\boldsymbol{b} = (b_x, b_y)$ in two dimension is defined by $\boldsymbol{a}\times\boldsymbol{b} = a_x b_y - a_y b_x$ and $b = a/\sqrt{3}$ is the equilibrium bond length. The dimensionless parameter β is given by

$$\beta = -\frac{\mathrm{d}\ln\gamma_0}{\mathrm{d}\ln b}, \tag{2.17}$$

where γ_0 is the resonance integral between nearest neighbor carbon atoms related to γ through $\gamma = (\sqrt{3}a/2)\gamma_0$. This means that the lattice distortion gives rise to a shift in the origin of the wave vector or an effective vector potential, i.e., u_x in the y direction and u_y in the x direction.

Explicitly, we have

$$\mathcal{H}_\mathrm{int} = -\sqrt{\frac{\hbar}{2NM\omega_0}} \sum_{\boldsymbol{q},\mu} \sqrt{2}\frac{\beta\gamma}{b^2} V_\mu(\boldsymbol{q}) \mathrm{e}^{\mathrm{i}\boldsymbol{q}\cdot\boldsymbol{r}} (b_{\boldsymbol{q}\mu} + b^\dagger_{-\boldsymbol{q}\mu}), \tag{2.18}$$

where

$$V^K_\mathrm{l}(\boldsymbol{q}) = \begin{pmatrix} 0 & -\mathrm{e}^{-\mathrm{i}\varphi(\boldsymbol{q})} \\ \mathrm{e}^{\mathrm{i}\varphi(\boldsymbol{q})} & 0 \end{pmatrix}, \tag{2.19}$$

and

$$V^K_\mathrm{t}(\boldsymbol{q}) = \begin{pmatrix} 0 & \mathrm{i}\mathrm{e}^{-\mathrm{i}\varphi(\boldsymbol{q})} \\ \mathrm{i}\mathrm{e}^{\mathrm{i}\varphi(\boldsymbol{q})} & 0 \end{pmatrix}, \tag{2.20}$$

for the K point. For the K' point, the corresponding quantities are obtained by the relation $V^{K'}_\mu(\boldsymbol{q}) = V^K_\mu(-\boldsymbol{q})^*$.

2.3 Phonon Green's Function

The phonon Green's function is written as

$$D_\mu(\boldsymbol{q},\omega) = \frac{2\hbar\omega_0}{(\hbar\omega)^2 - (\hbar\omega_0)^2 - 2\hbar\omega_0\Pi_\mu(\boldsymbol{q},\omega)}. \tag{2.21}$$

In the following, we shall consider retarded Green's function obtained by an analytic continuation of a thermal Green's function from upper complex plane. The phonon frequency is determined by the pole of $D_\mu(\boldsymbol{q},\omega)$ as

$$\Bigl(\frac{\omega}{\omega_0}\Bigr)^2 - 1 = \frac{2}{\hbar\omega_0}\mathrm{Re}\,\Pi_\mu(\boldsymbol{q},\omega). \tag{2.22}$$

As will become clear in the following, the phonon self-energy is small. In this case, the shift of the phonon frequency is given by

$$\Delta\omega_\mu = \frac{1}{\hbar}\mathrm{Re}\,\Pi_\mu(\boldsymbol{q},\omega_0), \tag{2.23}$$

and the broadening is given by

$$\Gamma_\mu = -\frac{1}{\hbar}\mathrm{Im}\,\Pi_\mu(\boldsymbol{q},\omega_0). \tag{2.24}$$

§3. Optical-Phonon Self-Energy

In the following we shall consider the phonons at the Γ point, i.e., $|\boldsymbol{q}| \to 0$ and the lowest order self-energy given by the diagram shown in Fig. 1. The matrix elements squared are independent of mode μ = t or l and K or K' points and given by

$$|(nX|V(\boldsymbol{q})|n'X)|^2 = |C_n|^2 |C_{n'}|^2 (\delta_{|n|,|n'|-1} + \delta_{|n'|,|n|-1}). \tag{3.1}$$

The self-energy is given by

$$\Pi(\boldsymbol{q},\omega) = -g_\mathrm{v} g_\mathrm{s} \Bigl(\frac{\beta\gamma}{b^2}\Bigr)^2 \frac{\hbar}{NM\omega_0} \sum_{n,n'} \sum_X |(nX|V(\boldsymbol{q})|n'X)|^2 \times \frac{f(\varepsilon_n) - f(\varepsilon_{n'})}{\hbar\omega - \varepsilon_n + \varepsilon_{n'} + \mathrm{i}0}, \tag{3.2}$$

where the subscript μ has been omitted, $f(\varepsilon)$ is the Fermi

distribution function,

$$f(\varepsilon) = \frac{1}{\mathrm{e}^{(\varepsilon-\zeta)/k_BT}+1}, \tag{3.3}$$

with ζ being the chemical potential, and g_v and g_s are the spin and valley degeneracy ($g_\mathrm{v}=g_\mathrm{s}=2$). Define the dimensionless coupling parameter

$$\lambda = \frac{g_\mathrm{v}g_\mathrm{s}}{4}\frac{36\sqrt{3}}{\pi}\frac{\hbar^2}{2Ma^2}\frac{1}{\hbar\omega_0}\Big(\frac{\beta}{2}\Big)^2. \tag{3.4}$$

For $M=1.993\times10^{-23}$ g, $a=2.46$ Å, and $\hbar\omega_0=0.196$ eV, we have

$$\lambda \approx 2.9\times10^{-3}\frac{g_\mathrm{v}g_\mathrm{s}}{4}\Big(\frac{\beta}{2}\Big)^2. \tag{3.5}$$

Then, we have

$$\Pi(\boldsymbol{q},\omega) = -2\lambda(2\pi\gamma^2)\frac{1}{2\pi l^2}\sum_{n,n'}|C_n|^2|C_{n'}|^2\delta_{|n|,|n'|-1} \times [f(\varepsilon_n)-f(\varepsilon_{n'})]\frac{2(\varepsilon_n-\varepsilon_{n'})}{(\hbar\omega+\mathrm{i}0)^2-(\varepsilon_n-\varepsilon_{n'})^2}. \tag{3.6}$$

This can be rewritten as

$$\Pi(\boldsymbol{q},\omega) = -\frac{1}{4}\lambda(\hbar\omega_B)^2\sum_{s,s'=\pm1}\sum_{n=0}^{\infty}[f(s\varepsilon_n)-f(s'\varepsilon_{n+1})] \times\frac{2(s\varepsilon_n-s'\varepsilon_{n+1})}{(\hbar\omega+\mathrm{i}0)^2-(s\varepsilon_n-s'\varepsilon_{n+1})^2}. \tag{3.7}$$

Consider the case of vanishing Fermi energy at zero temperature and in the limit of a weak magnetic field. Then, only inter-band processes contribute to $\Pi(\boldsymbol{q},\omega)$ and in the limit of $\omega\to0$, the self-energy becomes

$$\Pi^{\mathrm{2D}}(\boldsymbol{q},\omega) = \frac{1}{4}\lambda(\hbar\omega_B)^2\sum_{s,s'=\pm1}\sum_{n=0}^{\infty}\int_0^1\mathrm{d}t\ (1-ss') \times\frac{[f_0(s\varepsilon_{n+t})-f_0(s'\varepsilon_{n+t})]}{s\varepsilon_{n+t}-s'\varepsilon_{n+t}} = \frac{1}{4}\lambda(\hbar\omega_B)^2\sum_{s,s'=\pm1}\sum_{n=0}^{\infty}\frac{1-ss'}{\varepsilon_{n+1}+\varepsilon_n}, \tag{3.8}$$

with

$$f_0(\varepsilon) = \begin{cases} 0 & (\varepsilon>0);\\ 1/2 & (\varepsilon=0);\\ 1 & (\varepsilon<0). \end{cases} \tag{3.9}$$

The summation over n diverges and should be cutoff at n_c with $\varepsilon_n\sim\varepsilon_\mathrm{c}$ where ε_c is the cutoff energy of the order of the half of the π band width.

We are calculating the self-energy of optical phonons starting with the known phonon modes in graphene, which are usually calculated in an adiabatic approximation corresponding to $\omega\to0$. Therefore, this contribution $\Pi^{\mathrm{2D}}(\boldsymbol{q},\omega)$ is already included in the definition of ω_0. In order to avoid such a double-counting problem, we have to subtract $\Pi^{\mathrm{2D}}(\boldsymbol{q},\omega)$ from $\Pi(\boldsymbol{q},\omega)$. Thus, the final expression of the self-energy becomes

$$\Pi(\boldsymbol{q},\omega) = -\frac{1}{4}\lambda(\hbar\omega_B)^2\sum_{s,s'=\pm1}\sum_{n=0}^{\infty}\Big([f(s\varepsilon_n)-f(s'\varepsilon_{n+1})] \times\frac{2(s\varepsilon_n-s'\varepsilon_{n+1})}{(\hbar\omega+\mathrm{i}\delta)^2-(s\varepsilon_n-s'\varepsilon_{n+1})^2}-\frac{1-ss'}{\varepsilon_{n+1}+\varepsilon_n}\Big), \tag{3.10}$$

where we have introduced phenomenological broadening δ due to scattering of an electron by disorder or acoustic phonons. Note that this expression is free from the problem of divergence.

We have the relation

$$f_{-\zeta}(\varepsilon) = 1-f_\zeta(-\varepsilon), \tag{3.11}$$

which leads to the conclusion that the self-energy is symmetric between $\zeta>0$ and $\zeta<0$, i.e., the electron-hole symmetry. In the following, therefore, we shall confine ourselves to the case $\zeta>0$.

In the limit of vanishing magnetic field, we can set $\varepsilon_{n+1}\approx\varepsilon_n$ and replace the summation over n by an integral. Then, the above expression of the self-energy is reduced to the zero-field expression obtained previously.[3] At zero temperature, in particular, we have

$$\Pi(\boldsymbol{q},\omega) = \lambda\varepsilon_\mathrm{F} - \frac{1}{4}\lambda\,(\hbar\omega+\mathrm{i}\delta)\Big(\ln\frac{\hbar\omega+2\varepsilon_\mathrm{F}^0+\mathrm{i}\delta}{\hbar\omega-2\varepsilon_\mathrm{F}^0+\mathrm{i}\delta}+\pi\mathrm{i}\Big), \tag{3.12}$$

where ε_F^0 is the Fermi energy in the absence of a magnetic field. In the clean limit $\delta\to0$, the frequency shift, i.e., the real part, diverges logarithmically to $-\infty$ at $\varepsilon_\mathrm{F}^0=\hbar\omega_0/2$. Apart from this logarithmic singularity, the phonon frequency increases roughly in proportion to ε_F^0 for $\varepsilon_\mathrm{F}^0>\hbar\omega_0$. The broadening is nonzero and is independent of ε_F^0 for $\varepsilon_\mathrm{F}^0<\hbar\omega_0/2$ and vanishes for $\varepsilon_\mathrm{F}^0>\hbar\omega_0/2$.

The self-energy (3.10) shows that a resonance behavior appears when $\hbar\omega_B^{n\pm}=\hbar\omega_0$ with

$$\hbar\omega_B^{n\pm} = \hbar\omega_B\big(\sqrt{n+1}\pm\sqrt{n}\big). \tag{3.13}$$

The contribution of the resonance is given by

$$\frac{2\hbar\omega_B^{n\pm}}{(\hbar\omega_0+\mathrm{i}\delta)^2-(\hbar\omega_B^{n\pm})^2}\approx\frac{1}{\hbar\omega_0-\hbar\omega_B^{n\pm}+\mathrm{i}\delta}, \tag{3.14}$$

apart from a factor determined by the filling of the relevant Landau levels. The imaginary part has a Lorentzian peak and the real part exhibits a singularity $\sim(\omega_0-\omega_B^{n\pm})^{-1}$.

Such resonances can be classified into inter-band processes $\omega_B^{n+}\approx\omega_0$ and intra-band processes $\omega_B^{n-}\approx\omega_0$. The latter appears only in high magnetic fields at sufficiently high electron concentrations and the former appears in weak magnetic fields at low electron concentrations. Figure 2 shows some Landau levels $\pm\hbar\omega_B\sqrt{n}$ as a function of the effective magnetic energy $\hbar\omega_B$, together with the Fermi energy for a given electron concentration specified by zero-field Fermi energy ε_F^0. The resonance fields are specified by arrows connecting initial and final states.

As shown in Fig. 2(a), resonances due to transitions from $-n$ to $n+1$ and from $-n-1$ to n ($n>0$) disappear approximately for $\varepsilon_\mathrm{F}^0>(1/2)\hbar\omega_0$ and only the resonance from 0 to +1 and from −1 to 0 remains. As shown in Fig. 2(b), this resonance disappears when the Landau level $n=+1$ is fully occupied by electrons. With the use of the resonance condition $\omega_B^{0\pm}=\omega_0$, the resonance appears

when $0 < \varepsilon_{\rm F}^0/\hbar\omega_0 < \sqrt{3/2}$. In general, the resonance from n to $n+1$ ($n>0$) can appear in the concentration range where level n is occupied and level $n+1$ is not fully occupied. The condition is written as $\sqrt{n-(1/2)}(\sqrt{n}+\sqrt{n+1}) < \varepsilon_{\rm F}^0/\hbar\omega_0 < \sqrt{n+(3/2)}(\sqrt{n}+\sqrt{n+1})$. Figure 3 shows this energy range as a function of n. There is a certain gap in $\varepsilon_{\rm F}^0$ where no resonance occurs, but the gap decreases rapidly with n. It should be noted that the same gaps also appear in the cyclotron resonance.

§4. Numerical Results and Discussion

Figure 4 shows calculated frequency shift and broadening in the regime of low electron concentrations. At the lowest electron concentration $\varepsilon_{\rm F}^0/\hbar\omega_0 = 1/4$, all resonant transitions from $-n$ to $n+1$ and from $-n-1$ to n appear at $\omega_B^{n+} = \hbar\omega_0$. For $\varepsilon_{\rm F}^0/\hbar\omega_0 = 1/2$, contributions of transitions from $-n-1$ to n disappear because the Landau level n is fully occupied by electrons at resonances. For $\varepsilon_{\rm F}^0/\hbar\omega_0 = 3/4$, only the resonant transition from 0 to 1 remains.

Figure 5 shows the phonon spectral function $(-1/\pi)$ Im$D(\boldsymbol{q},\omega)$. At resonances, the phonon spectrum exhibits characteristic behavior and the phonon practically disappears due to large broadening at a magnetic field corresponding to the exact resonance.

Figure 6 shows the frequency shift and broadening of optical phonon in the regime of high electron concentrations where intra-band resonances can appear. As is shown in Fig. 3, no resonance can take place for $\varepsilon_{\rm F}^0/\hbar\omega_0 = 1.5$ and both shift and broadening do not exhibit singular structure except for a small cusp and dip due to sudden jumps of the Fermi level between Landau levels. For $\varepsilon_{\rm F}^0/\hbar\omega_0 = 2.5$ and 4.5, a resonance occurs from 1 to 2 and from 2 to 3, respectively. For $\varepsilon_{\rm F}^0/\hbar\omega_0 = 3.825$ lying in the gap shown in Fig. 3, no exact resonance can occur and both shift and broadening exhibit complicated dependence on the magnetic field.

In Fig. 6, the frequency shift in the weak field region $\hbar\omega_B \sim \hbar\omega_0$ increases roughly in proportion to $\varepsilon_{\rm F}^0$. This corresponds to the previous result in the absence of a magnetic field given in eq. (3.12).[3] Similar behavior is apparent also in Fig. 4. In fact, the frequency shift at $\hbar\omega_B/\hbar\omega_0 \sim 0.1$ is negative and its absolute value increases with the decrease of $\delta/\hbar\omega_0$ for $\varepsilon_{\rm F}^0/\hbar\omega_0 = 1/2$, corresponding to the logarithmic singularity. Further, the broadening in the weak-field region disappears for $\varepsilon_{\rm F}^0/\hbar\omega_0 > 1/2$.

The effective magnetic energy $\hbar\omega_B$ is given by

$$\hbar\omega_B = \frac{\sqrt{2}\gamma}{l} = 35.6 \times \frac{\gamma\,[\text{eV}\cdot\text{Å}]}{6.46}\sqrt{B\,[\text{T}]}\ \text{meV}, \qquad (4.1)$$

For the parameter $\gamma = 6.46$ eV·Å giving $\gamma_0 = 3.03$ eV and $\hbar\omega_0 = 196$ meV corresponding to 1583 cm^{-1}, we have $B_0 = 30.1$ T corresponding to $\hbar\omega_B = \hbar\omega_0$. The electron concentration corresponding to the condition $\varepsilon_{\rm F}^0 = \hbar\omega_0/2$ becomes 0.73×10^{12} cm^{-2}. For the mobility of $\mu \sim 10^4$ cm^2/Vs, the broadening in the absence of a magnetic field becomes $\hbar/\tau$ becomes ~ 6 meV, where use has been made of $\mu = ev^2\tau/\varepsilon_{\rm F}$ with $v = \gamma/\hbar$.[16] Actual broadening is likely to be larger than this estimated value because the transport relaxation time can be longer than the conventional relaxation time giving the broadening of the spectral function. In ref. 6 this factor has been shown to be two for scatterers with potential range smaller than the Fermi wavelength.

The broadening of Landau levels was shown to be given by $\Gamma_n = \hbar\omega_B\sqrt{(1+\delta_{n0})W}$, where W is the dimensionless parameter characterizing the strength of scattering, $W \approx \hbar/2\pi\varepsilon_F^0\tau$.[6,7] By assigning $\delta \approx \Gamma_N$ with $\varepsilon_F^0 = \hbar\omega_0/2$, we have $W \approx \hbar/2\pi\varepsilon_F^0\tau \sim 0.01$. It is possible, therefore, to observe the anomaly of optical phonons due to inter-band resonances. For the observation of effects of intra-band resonances, much higher magnetic field reachable only by pulse magnets is required although the electron concentration is within accessible range.

§5. Summary and Conclusion

In this paper, the energy shift and broadening of optical phonons have been calculated in a monolayer graphene in magnetic fields. Both frequency shift and broadening exhibits a singular behavior when resonance occurs between Landau levels. The selection rules for the resonance are the same as those for optical transitions. Resonances corresponding to inter-band transitions are expected to be observed at low electron concentrations in high-mobility systems.

Acknowledgments

This work was supported in part by a 21st Century COE Program at Tokyo Tech "Nanometer-Scale Quantum Physics" and by Grant-in-Aid for Scientific Research from Ministry of Education, Culture, Sports, Science and Technology Japan.

References

1) A. C. Ferrari, J. C. Meyer, V. Scardaci, C. Casiraghi, M. Lazzeri, F. Mauri, S. Piscanec, D. Jiang, K. S. Novoselov, S. Roth, and A. K. Geim: Phys. Rev. Lett. **97** (2006) 187401.
2) A. Gupta, G. Chena, P. Joshi, S. Tadigadapa, and P. C. Eklund: cond-mat/0606593.
3) T. Ando: J. Phys. Soc. Jpn. **75** (2006) 124701.
4) J. W. McClure: Phys. Rev. **104** (1956) 666.
5) T. Ando: J. Phys. Soc. Jpn. **74** (2005) 777.
6) N. H. Shon and T. Ando: J. Phys. Soc. Jpn. **67** (1998) 2421.
7) Y. Zheng and T. Ando: Phys. Rev. B **65** (2002) 245420.
8) T. Ando, Y. Zheng, and H. Suzuura: J. Phys. Soc. Jpn. **71** (2002) 1318.
9) T. Ando, A. B. Fowler, and F. Stern: Rev. Mod. Phys. **54** (1982) 437 and references cited therein.
10) K. S. Novoselov, A. K. Geim, S. V. Morozov, D. Jiang, Y. Zhang, S. V. Dubonos, I. V. Grigorieva, and A. A. Firsov: Science **306** (2004) 666.
11) K. S. Novoselov, A. K. Geim, S. V. Morozov, D. Jiang, M. I. Katsnelson, I. V. Grigorieva, S. V. Dubonos, and A. A. Firsov: Nature **438** (2005) 197.
12) Y. Zhang, Y.-W. Tan, H. L. Stormer, and P. Kim: Nature **438** (2005) 201.
13) V. P. Gusynin and S. G. Sharapov: Phys. Rev. Lett. **95** (2005) 146801.
14) N. M. R. Peres, F. Guinea, and A. H. Castro Neto:

Phys. Rev. B **73** (2006) 125411.
15) H. Kumazaki and D. S. Hirashima: J. Phys. Soc. Jpn. **75** (2006) 053707.
16) T. Ando: J. Phys. Soc. Jpn. **75** (2006) 074716.
17) I. F. Herbut: Phys. Rev. Lett. **97** (2006) 146401.
18) V. M. Pereira, F. Guinea, J. M. B. Lopes dos Santos, N. M. R. Peres, and A. H. Castro Neto: Phys. Rev. Lett. **96** (2006) 036801.
19) D. V. Khveshchenko: Phys. Rev. Lett. **97** (2006) 036802.
20) E. McCann, K. Kechedzhi, V. I. Falko, H. Suzuura, T. Ando, and B. L. Altshuler: Phys. Rev. Lett. **97** (2006) 146805.
21) Y. Zhang, Z. Jiang, J. P. Small, M. S. Purewal, Y.-W. Tan, M. Fazlollahi, J. D. Chudow, J. A. Jaszczak, H. L. Stormer, and P. Kim: Phys. Rev. Lett. **96** (2006) 136806.
22) S. V. Morozov, K. S. Novoselov, M. I. Katsnelson, F. Schedin, L. A. Ponomarenko, D. Jiang, and A. K. Geim: Phys. Rev. Lett. **97** (2006) 016801.
23) H. Suzuura and T. Ando: Phys. Rev. B **65** (2002) 235412.
24) K. Ishikawa and T. Ando: J. Phys. Soc. Jpn. **75** (2006) 084713.
25) P. R. Wallace: Phys. Rev. **71** (1947) 622.
26) G. S. Painter and D. E. Ellis: Phys. Rev. B **1** (1970) 4747.
27) J. C. Slonczewski and P. R. Weiss: Phys. Rev. **109** (1958) 272.
28) H. Ajiki and T. Ando: J. Phys. Soc. Jpn. **62** (1993) 1255.

Figure Captions

Fig. 1 A Feynman diagram for the self-energy of optical phonons with wave vector $\boldsymbol{q}$ and Matsubara frequency ω_m.

Fig. 2 The Landau levels (thin dotted lines) as a function of effective magnetic energy $\hbar\omega_B \propto \sqrt{B}$ and the Fermi energy for a given electron concentration characterized by the Fermi energy $\varepsilon_{\rm F}^0$ in the absence of a magnetic field. The vertical arrows show transitions at a resonance. (a) Low electron concentrations. (b) High electron concentrations.

Fig. 3 The range of the Fermi energy where the resonance from n to n+1 occurs as a function of n ($n>0$) and the gap where no resonance occurs.

Fig. 4 The frequency shift (solid line) and broadening (dashed line) of optical phonons as a function of effective magnetic energy $\hbar\omega_B$ at low electron concentrations corresponding to inter-band resonances. Thin vertical lines show resonance magnetic fields. (a) $\varepsilon_{\rm F}^0/\hbar\omega_0 = 1/4$, (b) 1/2, and (c) 3/4. The results for $\delta/\hbar\omega_0 = 0.1$, 0.05, and 0.02 are shown.

Fig. 5 The phonon spectral function $(-1/\pi){\rm Im}D(\boldsymbol{q},\omega)$ for (a) $\varepsilon_{\rm F}^0/\hbar\omega_0 = 1/4$, (b) 1/2, and (c) 3/4. $\delta/\hbar\omega_0 = 0.05$. The dotted line shows the frequency shift, i.e., the peak position, as a function of $\hbar\omega_B$.

Fig. 6 The frequency shift (solid line) and broadening (dashed line) of optical phonons as a function of effective magnetic energy $\hbar\omega_B$ at high electron concentrations corresponding to intra-band resonances. The vertical straight lines show the effective magnetic field corresponding to resonances $+1 \to +2$, $+2 \to +3$, and $+3 \to +4$. No resonance occurs for $\varepsilon_{\rm F}^0/\hbar\omega_0 = 3.825$. $\delta/\hbar\omega_0 = 0.05$.

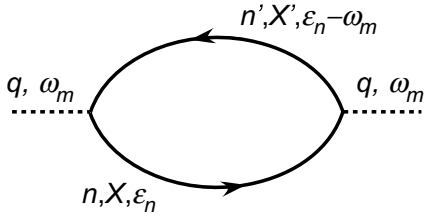

Fig. 1

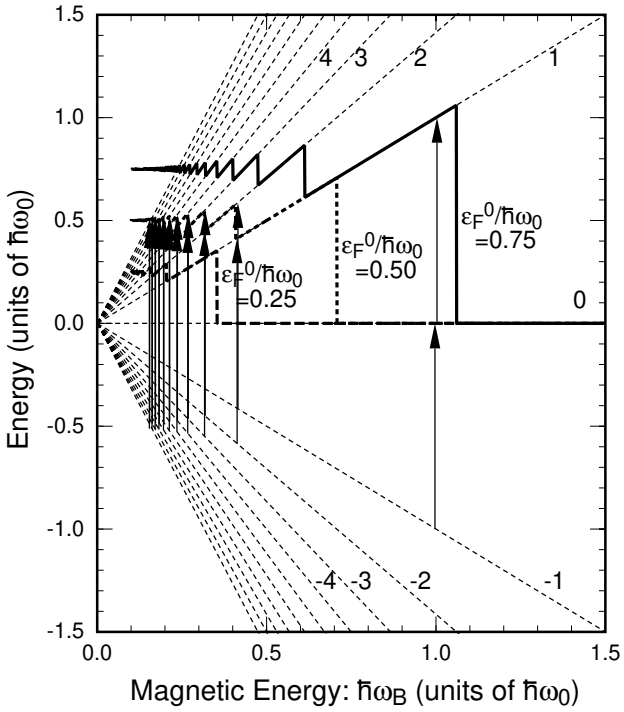

Fig. 2(a)

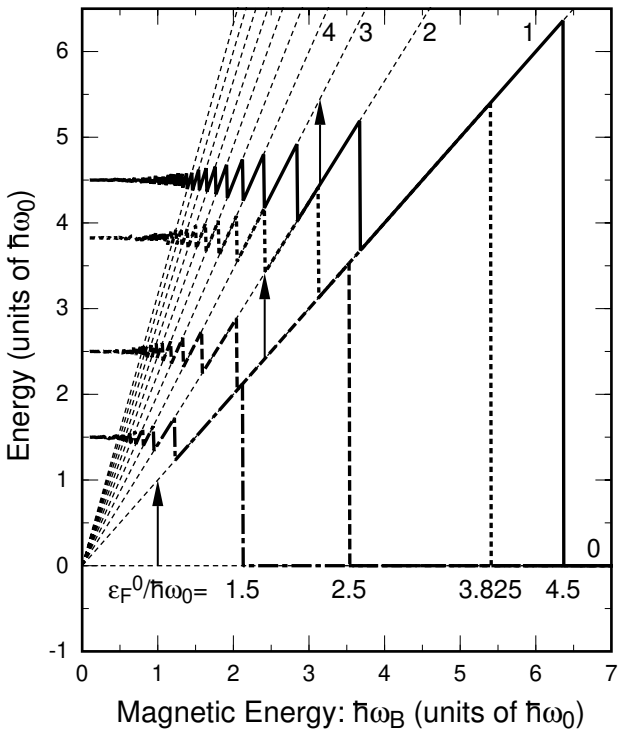

Fig. 2(b)

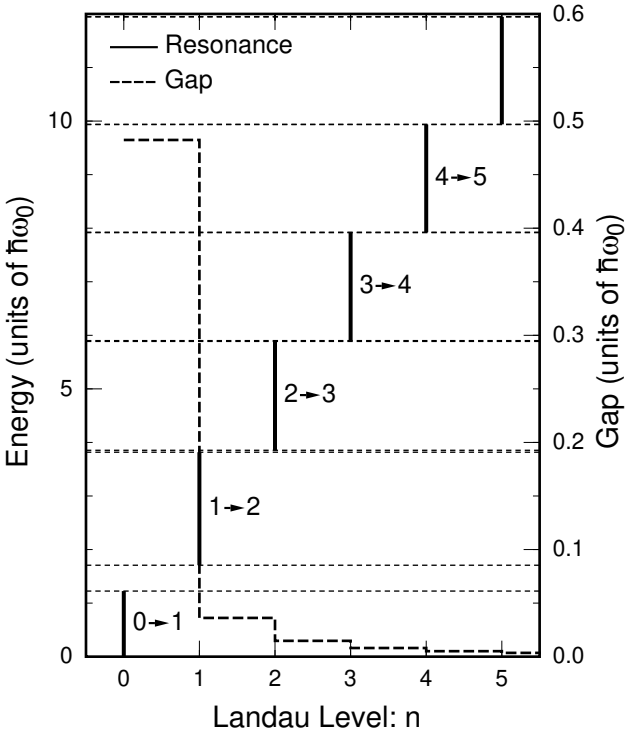

Fig. 3

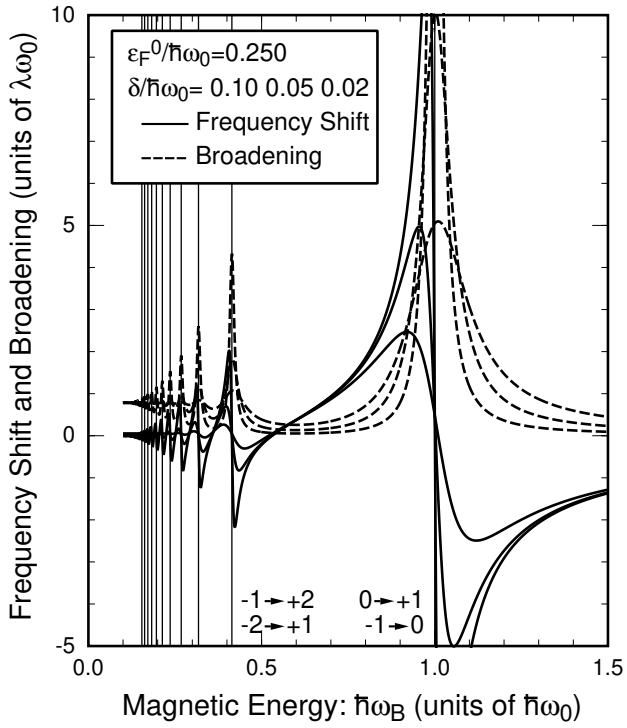

Fig. 4(a)

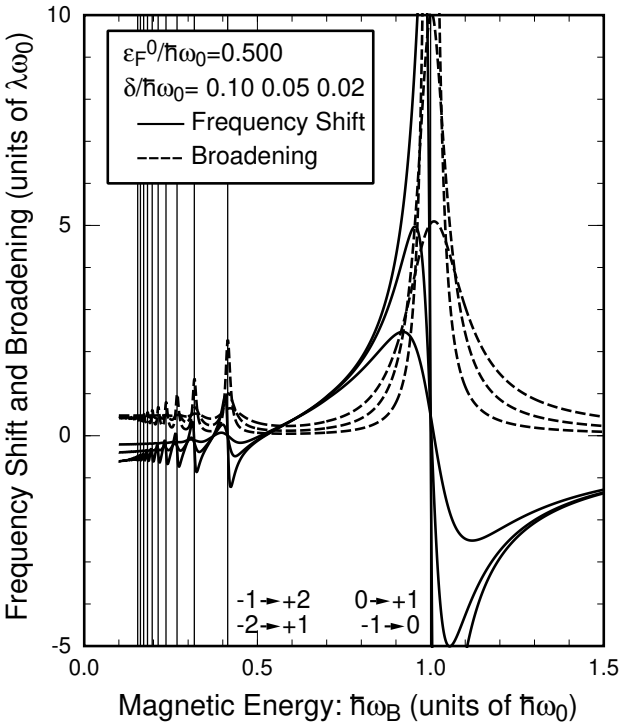

Fig. 4(b)

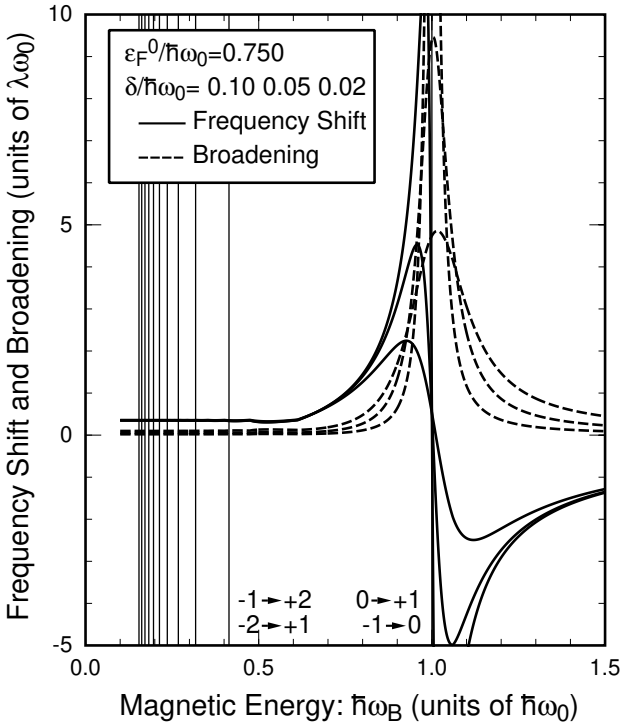

Fig. 4(c)

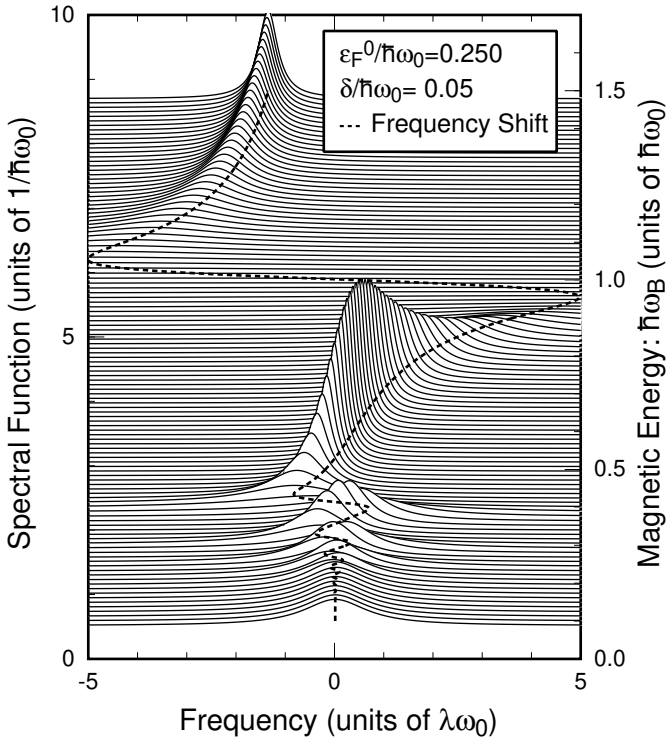

Fig. 5(a)

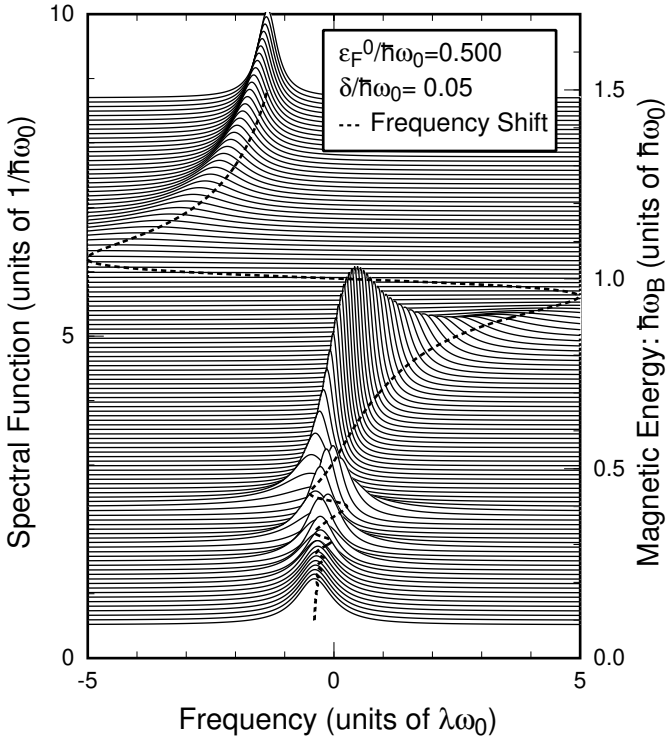

Fig. 5(b)

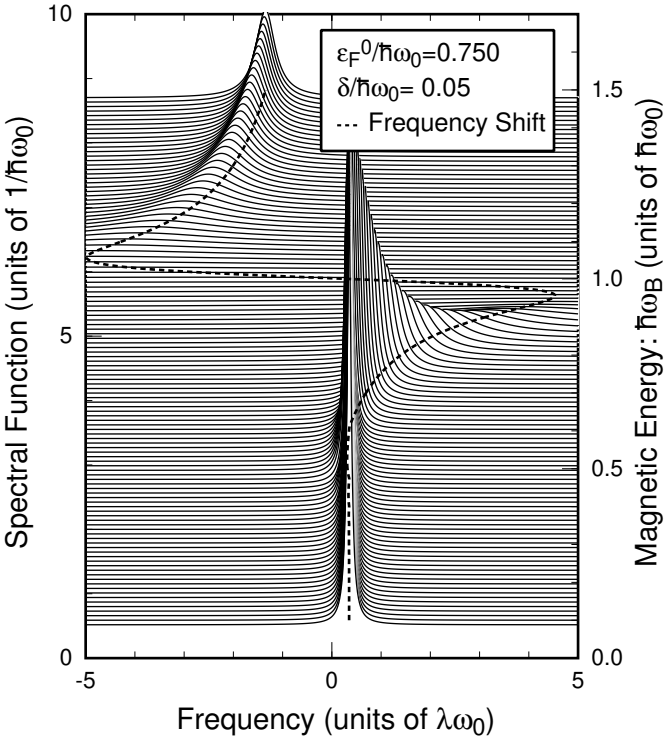

Fig. 5(c)

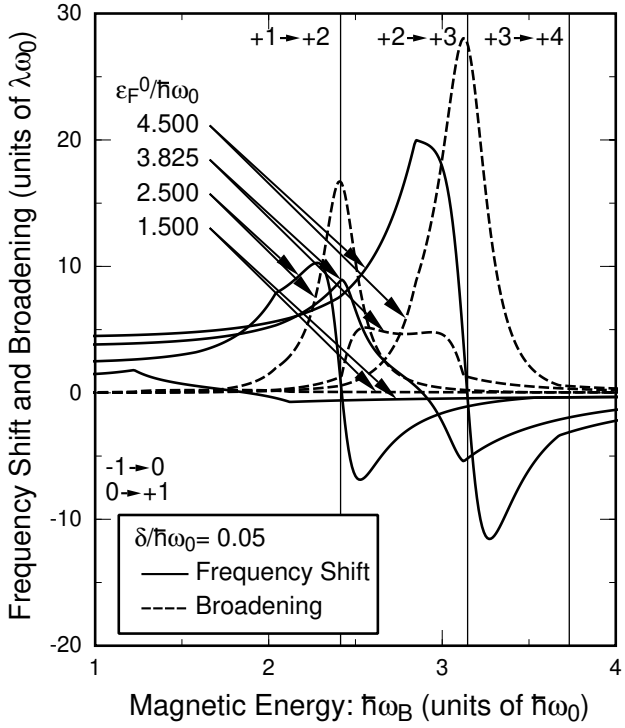

Fig. 6